Femtosecond pulse jitter measurements using sum frequency generation

Master's thesis
by
Måns Schultz

Lund reports on Atomic Physics, LRAP 364
Lund, June 2006

Abstract

One of the steps in the continuing process to develop free electron lasers is the development of a system for timing of probe and pulse pulses. A method for measuring jitter between two femtosecond light pulses was developed using a Ti:Sa laser and self-phase modulation in glass which simulated the conditions of the Tesla test facility (TTF) at Desy, Hamburg. Two 600 and 790 nm pulses generated a 340 nm pulse in a KDP crystal which was depicted onto a detector. Several detectors were tested and a final setup which can measure the delay with better than 100 fs accuracy for photons counts of 10^6 600 nm photons/pulse was developed.

Contents

Chapter 1

Introduction

The purpose of this diploma work is to develop a method to measure the temporal delay between two femtosecond light pulses with different wavelengths and photon counts using sum frequency generation of 790 and 600 nm beams. The setup should be cheap, have a good accuracy and be able to handle very low 600 nm photon counts.

1.1 The need for free electron lasers

The range of applications for free electron lasers is very large and listing them all is beyond this report. A free electron laser is basically a super bright tunable laser source that can access wavelength regions where there are few traditional laser system. One of the more significant applications is the generation of high intensity ultrashort x-ray pulses. Creating a x-ray laser using conventional laser technology is a problem for several reasons. First normal multi pass lasers use optics to make the beam pass several time through an amplification media. Even if x-ray optics do exist it is very hard to create a cavity with the same efficiency as for longer wavelengths [1] Furthermore a normal system that depends on stimulated emission has problems at shorter wavelengths since the rate of spontaneous to stimulated emission is proportional to the frequency to the power of three. This means that as shorter wavelengths it is hard to get the cascading emission that generates a strong and short laser pulse. However as described below the frequency of FELs are only depend on the electron beam energy and wiggler frequency and have no problem scaling up to high frequencies.

A strong x-ray laser has the possibility to study femtosecond chemical processes and structural biology [2]. This would for example make it possible to take a snapshot of viral attacks on a cell in atomic detail [3]. In theory any chemical reactions could be recorded as a film and analyzed. Other applications include atomic cluster studies for nanotechnology and plasma creation.

1.2 The need for jitter measurements

"Jitter" is often used as a term to describe the relatively small short term delay changes between two pulses. One obvious reason to measure this jitter is that it can be used to diagnose the FEL pulses. If a reliable optical laser is available this can be used as a reference. There are however other methods for doing this. The main reason one would want to measure the jitter between two pulses is that many experiments use the so called pump/probe method. This means that two beams are used for experiments. First the sample is excited to the desired state by the pump pulse and secondly the excited sample is probed by the probe pulse. Of course it is vital that the probe pulse arrives at the right time after the pump pulse. This is where jitter measurements become important.

So what causes jitter? In a big facility like a FEL the two laser systems might be quite some distance apart. Thermal expansion during the day and vibrations in the ground in the scale of tens of micrometers is enough to shift a fs laser pulse by its own length. Also there may be energy variations from electron bunch to bunch in the accelerator which can lead to jitter. And of course jitter measurements are needed for alignment.

Chapter 2

Free electrons lasers

Although it has been almost 35 years [3] since the construction of the first Free Electron Laser (FEL) it remains an active and largely unexplored field of science. This is mainly due to the fact that new accelerators have opened the possibility of operating a FEL at very short wavelengths ($\sim 0.1nm$) where there are few sources of bright, coherent, narrow bandwidth light. The possibility to combine the penetrating power of x-rays with the properties of a laser is what drives the X-ray FEL (hence X-FEL) research. For a more complete theory of FEL see [4].

2.1 Theory overview

The main difference between a normal laser and a FEL is the active media. In a normal laser the atoms are excited and the laser radiation comes from stimulated emission from some long-lived excited state. In a FEL however the active media is an electron beam that travels through a series of magnets called an *undulator* with alternating poles as shown in picture 2.1.

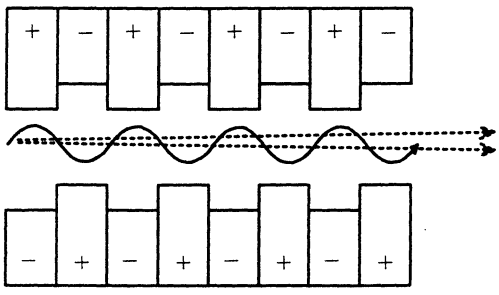

Figure 2.1: Basic principle of a FEL: An electron beam moving in an undulator.

As the electrons travel through the magnetic field they will subject to a periodic potential forcing them to move in a wavelike motion. As changed particles, every time the electrons are subject to a force which change their trajectory they emit light known as *synchrotron radiation.* If the electrons travel at relativistic speeds this radiation will, viewed from a system at rest with respect to the undulator, be emitted in a cone as seen in figure 2.1. Note that the radiation emitted in this way is incoherent and can hardly be called a laser source on its own. This can be compared to the spontaneous emissions of a normal laser. Sometimes a laser beam is injected into the electron cavity to accelerate the process. In the first case the FEL is called a *Self Amplified Spontaneous Emission Free Electron Laser* or *SASE-FEL.* Since light is emitted at every turn the electron is forced to take this light will interfere with itself to create a spectra of wavelengths. To simplify things we assume that the higher order harmonics can be neglected. The primary wavelength emitted by a FEL along the path of the electron beam is given as in [5]

$$\lambda_{FEL} = \frac{\lambda_u}{2\gamma^2}(1 + \frac{K^2}{2}) \tag{2.1}$$

where λ_u is the undulator wavelength, γ the electron energy and K the undulator strength parameter. As the strength of the optical field grows the electrons will after a while start to interact with the optical field. First we shall study only a single electron. Depending on the relative phase between the electron and the optical field the electrons will in their sinusoidal motion experience either an retarding or accelerating force from the optical field. This in turn will lead to that the electron beam either loose or gain energy from the optical field depending on their relative phase.

This can be derived from the Lorentz force equation:

$$\frac{\Delta \mathbf{p}}{\Delta t} = e(\mathbf{E} + (\mathbf{v}/c) \times \mathbf{B}) \tag{2.2}$$

Consider a system where the undulator field axis is in the y-plane and the electrons are traveling along the z-axis. By assuming that the undulator field does not vary in time and that all waves behave like plane waves the change in electron energy along the axis of the undulator (here the z-axis) can be derived as [6]

$$\frac{\Delta \gamma}{\Delta z} = -\frac{w_o a_o a_u}{2c\gamma} sin(\theta) \tag{2.3}$$

where γ is the electron energy, a_u and a_o the scaled vector potentials for the undulator and optical fields $a_n = \frac{e}{mc^2} A_n$ ($A_o = \frac{E_{ox} c}{w_o}$ and $A_u = \frac{B_{uy}}{k_u}$), w_o the optical field angular frequency and k_u the wavenumber of the undulator

magnetic field. The last term $\theta = (k_o + k_u)z - w_o t + \phi_o + \phi_u$ is known as the *ponderomotive phase* and describes the electrons position relative to the undulator and optical fields and the entire right side of the equation describes the *ponderomotive force* which in turn gives rise to the periodic *ponderomotive potential.* Actually if one studies the equations that govern the change in ponderomotive phase and energy further they describe the model of a pendulum. Since the electrons can never become fully relativistic the optical field will travel over them as they move through the undulator. The electron are said to *slip* back. If the ponderomotive phase is 0 then the slippage is constant that is the electron will feel the same force from the optical field in every oscillation. At this energy the electrons are said to be in *resonance* or have *resonance energy.* In resonance the net gain of the FEL is 0. However by controlling the electron beam energy one can control the equilibrium position. If the electron beam energy is higher than the resonance energy the system will experience a net gain. This is done by matching the speed of the ponderomotive wave such that it is slightly slower than the electrons, that is the electrons have a slightly higher energy than the resonance energy. When then electron looses energy to the optical field in this way the FEL is said to operate in the *low gain* region.

However the trajectory of the electron moving in an undulator is highly dependent on its energy. A electron with high energy will move in almost a straight line and an electron with lower energy will have a stronger oscillating motion. As the oscillating motion takes a longer path than the straight motion electrons with lower energy will start to lag behind. This will in turn affect their ponderomotive phase. So an electron which initially looses energy to the optical field will lag behind until it is in a position in which it gain energy and the other way around. In this way the ponderomotive potential will try to force electron into a phase where they are in equilibrium. As as the strength of the optical field grows this effect will get stronger and stronger. This is called *phase bunching.*

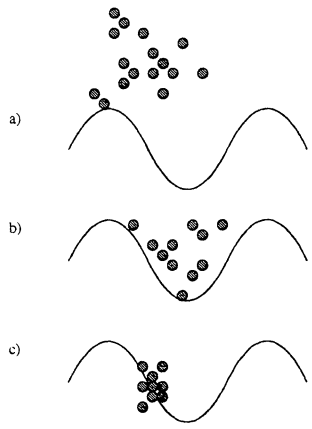

Figure 2.2: The electron phase and energy under the influence of the ponderomotive force at the different stages of FEL operation: a) Low gain regime b) High gain regime c) Complete phase bunching and saturation.

If the beam energy is above resonance then the electrons will then be bunched in a phase where they are constantly giving energy to the optical field. Since the electrons are bunched they will now all emit light at the same time, creating a very

strong optical field which further bunches the beam. This is called the *high gain* region. The FEL is now a very bright coherent laser source which can emit a pulse train of very short pulses at the desired wavelength.

2.2 Detector implementation

To measure the jitter using the main x-fel pulse directly introduces several problems. Since the pulse should be used for experiments only a part of it should be used for correlation. This introduces the problem of constructing very durable xray optics that isnt damaged by the main pulse. An easier way is to use light emitted from the beam dump. When the electron beam is bent off it will send out synchrotron radiation in a wide spectra. It is a part of this spectra that this experiment simulates using white-light generation. Since this radiation will be correlated with the electron bunches which in turn is in sync with the main x-ray beam this will effectively measure the jitter of the main x-ray beam. The optical laser is assumed to operate in a region where suitable optics are available, in this experiment this laser is a 790 nm Ti:Sa laser.

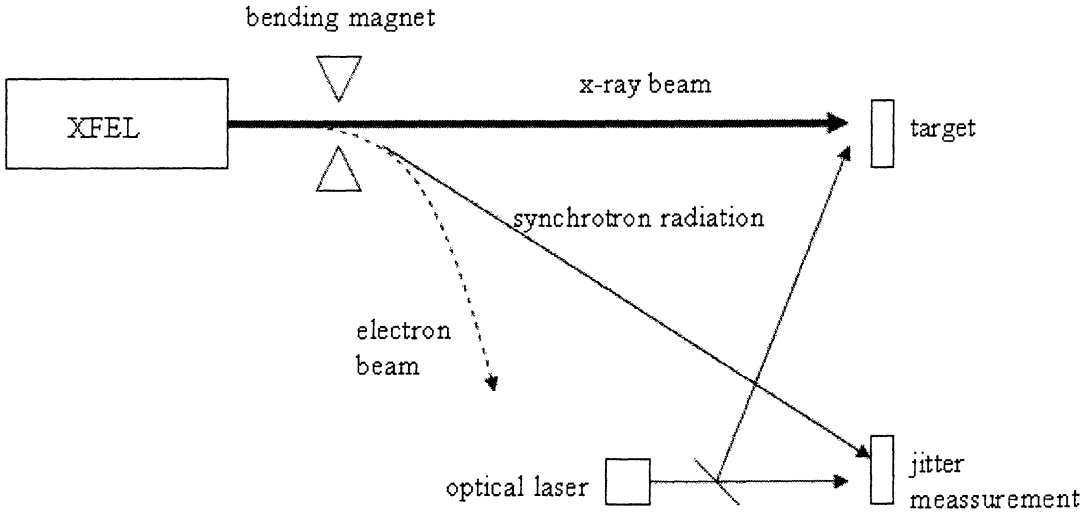

Figure 2.3: A suggestion for FEL jitter measurement implementation

Chapter 3

Nonlinear processes

For a proper understanding of the experiment some basic optics and atomic physics theory is needed. This is needed to explain how the test-setup was designed and how the technique for measuring the delay works.

3.1 Basics

Modern light sources such as Ti:Sa lasers can achieve high peak intensities at which the traditional models which govern radiation and its interaction with matter have to be modified. The general term for effects that appear at higher intensities is *non-linear effects.*
These changes in physical properties will in turn give rise to a number of measurable phenonomen. The effects described here are intensity dependent refractive indexes, giving rise to *white light generation* and non-linear polarization that leads to *sum frequency generation.* For a more complete review of the field see [7]. At the end the cross correlation principle is mentioned.

3.2 Sum frequency generation

The polarization of any media can be described as a Taylor expansion of the electric field

$$P = \chi_1 E + \chi_2 E^2 + \ldots + \chi_n E^n \tag{3.1}$$

However normally all terms except the first one can be neglected leading to the known equation

$$P = \chi_1 E \tag{3.2}$$

but at sufficiently high electric fields ($\sim 10^{11} V/m$ [8]), and thus high intensities since $I \sim E^2$, this is no longer a valid approximation and the second

term has to be included as well. This term is called the *nonlinear response* of the material.

Consider the nonlinear response of a material under the influence of two light beams with frequencies ω_1 and ω_2. The resulting electric field can be written as

$$E_{tot}(t) = E_1 e^{i\omega_1 t} + E_2 e^{i\omega_2 t} + c.c. \tag{3.3}$$

and the nonlinear polarization

$$P^2 = \chi_2 E_{tot}^2 = \chi_2 \underbrace{(E_1^2 e^{2i\omega_1 t} + E_2^2 e^{2i\omega_2 t}}_{Second-harmonicgeneration} + \underbrace{2E_1 E_2 e^{i(\omega_1+\omega_2)t}}_{sum-frequencygeneration} + \tag{3.4}$$
$$\underbrace{2E_1\overline{E_2}e^{i(\omega_1-\omega_2)t}}_{difference-frequencygeneration} + c.c.) + \chi_2 \underbrace{(2E_1\overline{E_2} + 2\overline{E_1}E_2}_{opticalrectification} + c.c.)$$

where the terms represent the different non-linear effects. In this experiment we are only interested in the sum-frequency generation term. The amplitude of this effect is proportional to the product of the electric field of the two beams. Thus a stronger pulse will induce more sum-frequency photons. However these equations tell us nothing of the conditions under which these effects become observable or of their individual conversion efficiencies. A complete explanation [7] is beyond this report, we will give a quick review of the simplest and strongest contributing factor.

Consider the sum-frequency generation processes as an addition of wave vectors. The incoming light has is represented as wave vectors $\vec{k_1}$ and $\vec{k_2}$ and the generated wave as $\vec{k_3}$ with corresponding wave numbers $k = \frac{n_\omega \omega}{c}$. Conservation of momenta state that

$$k_1 + k_2 = k_3 \tag{3.5}$$

which can be rewritten as

$$\omega_1 n(\omega_1)\cos\phi_1 + \omega_2 n(\omega_2)\cos\phi_2 = \omega_3 n(\omega_3) \tag{3.6}$$
$$\omega_1 n(\omega_1)\sin\phi_1 + \omega_2 n(\omega_2)\sin\phi_2 = 0 \tag{3.7}$$

Where ϕ_1 and ϕ_1 are the angle between the incoming beams and the generated beam in the crystal as shown in picture 3.2. Note that if the crystal in placed in air the beams will be refracted in its surface at the angles have to be recalculated. Whenever ϕ_1 and ϕ_2 are mentioned in this report they are referring to the angles inside the crystal.

In most materials it is not possible for equation 3.6 to hold and these effects are not observable. These equations are generally known as the *phase-matching condition* for sum frequency generation. For the highly simplified case of $\omega_1 = \omega_2 = \omega$ and $\phi_1 = \phi_2 = 0$ this simplifies into

$$n_{2\omega} = n_\omega \tag{3.8}$$

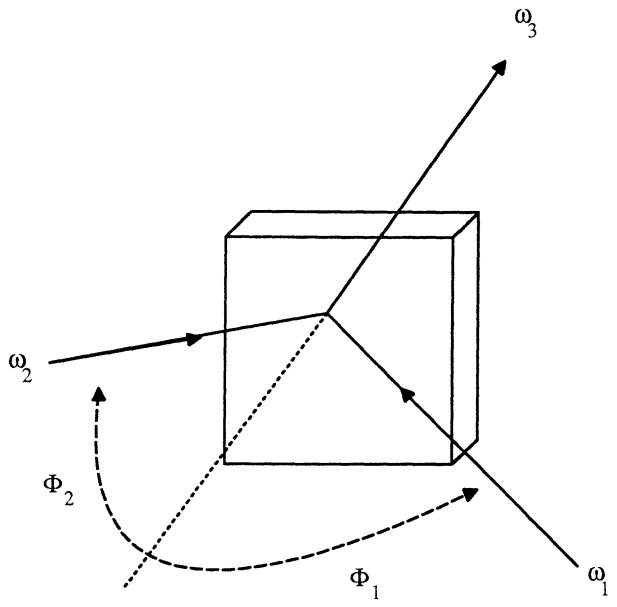

Figure 3.1: Sum frequency generation in a birefringent material

However almost all materials have a refractive index that varies with ω. Since χ_2 is 0 for centrosymmetric materials [8] we would expect a media where sum-frequency generation takes place to be optically anisotropic. This means that the refractive index will vary not only with ω but also with the polarization of the photons. Such materials are called *birefringent* and have two refractive indexes, one for polarizations parallel to the optical axis (n_o) of the material and one for polarizations perpendicular to it (n_e). Consider an incoming photon entering a birefringent material. Divide the polarization vector of incoming photon into two components, one component in a plane perpendicular to the optical axis of the material and the second perpendicular to the first. The first component, called the *ordinary* component always feels the same refractive index no matter which direction the light is propagating in. The other component called the *extraordinary* component will feel a refractive index that depends on the angle the photon is traveling in compared to the optical axis of the material described by:

$$n_e(\theta)_{effective} = \sqrt{\frac{n_o^2 n_e^2}{n_o^2 \cos\theta^2 + n_e^2 \sin\theta^2}} \tag{3.9}$$

Where θ is the angle between the line of propagation of the photon and the optical axis of the material. The type of phasematching used is this experiment is called *type 1 critical phasematching* the incoming waves are both ordinary while the sum-frequency wave is extraordinary. The trick is

the to find an angle θ such that equation 3.6 holds. Equation 3.6 then transforms to

$$\omega_1 n_o(\omega_1)\cos\phi_1 + \omega_2 n_o(\omega_2)\cos\phi_2 = \omega_3 n_e(\omega_3,\theta) \quad (3.10)$$

$$\omega_1 n_o(\omega_1)\sin\phi_1 + \omega_2 n_o(\omega_2)\sin\phi_2 = 0 \quad (3.11)$$

combining these equations with equation 3.9 enables us to calculate the phasematch angle for sum-frequency generation.

$$\theta = \arcsin\sqrt{\frac{(\frac{n_o(w_3)\omega_3}{\cos\phi_1 n_o(\omega_1)\omega_1+\cos\phi_2 n_o(\omega_2)\omega_2\omega_3})^2-1}{(\frac{n_o(w_3)}{n_e(w_3)})^2-1}} \quad (3.12)$$

3.3 White light generation

As mentioned earlier white light generation is a consequence of the fact that the refractive index of a medium at high intensities becomes a function of the intensity. This is called the *Optical Kerr effect*

$$n(I) = n_0 + n_1 I + \ldots \quad (3.13)$$

The shift in refractive index can be observed in [9]

$$\delta n = \frac{2\pi}{n_0}\delta\chi \quad (3.14)$$

$$\delta\chi(t) = \chi_3 I_\omega \quad (3.15)$$

where χ_3 is taken from equation 3.1. Here it is the shape of the pulse that determines the spectral broadening as much as the properties of the material.

A change in refractive index will induce a phase shift in the pulse. However since a pulse is not constant in intensity over time and the refractive index has become intensity dependent this means that not all parts of the pulse will experience the same phase shift. And since the frequency of the wave depends on the derivate of the phase

$$\omega = \omega_0\frac{\delta(\Delta\phi)}{\delta t} \quad (3.16)$$

the pulse will be spectrally broadened [9]

$$\delta\omega = -\frac{\delta(\Delta\phi)}{\delta t} = -\frac{2\pi\omega_0^2}{c^2 k_0}\chi_3\frac{\delta I}{\delta t}z \quad (3.17)$$

For strong focused femtosecond pulses with very high peak intensities this broadening will get so large that the the pulse will contain a large part of the visible spectra and thus look white. Hence *white-light generation*, the general process of frequency modulation is called *self-phase modulation.*

3.4 Cross correlation principle

Consider two light pulses entering a birefringent material. If the crystal is turned in the appropriate angle for phasematching the beams can form a third sum-frequency beam. However if the pulses are sufficiently short, this interaction will only take place in parts of the crystal.

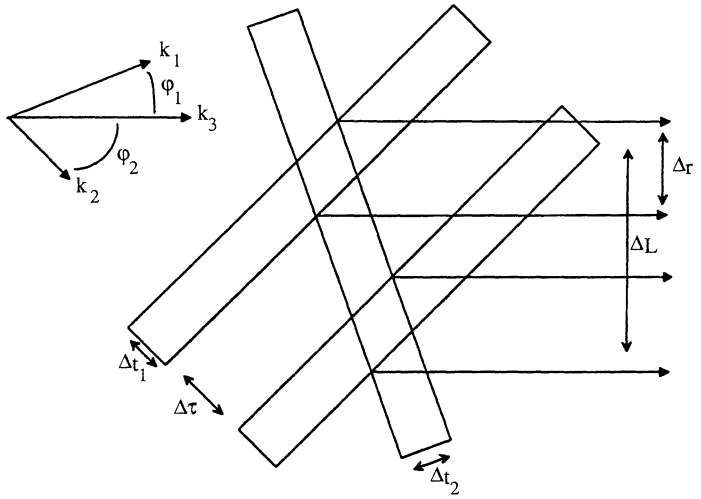

Figure 3.2: Crosscorrelation in a birefringent material

Depending on the relative delay between the pulses the position where the beams meet change. This is turn will change the position where the sum frequency beam is generated. This can be used to determine the temporal delay between the pulses as the delay will lead to a shift in position of the area where the beams interact. The sum frequency beam size δr and the resulting shift in position δL caused by a time delay $\delta\tau$ can be expressed as follows:

$$\Delta r = \frac{\frac{\cos(\varphi_1)\Delta t_2 c}{n_2} + \frac{\cos(\varphi_2)\Delta t_1 c}{n_1}}{\sin(\varphi_1+\varphi_2)} \tag{3.18}$$

$$\Delta L = \frac{\Delta\tau c}{\cos(\frac{\varphi_1+\varphi_2}{2})n_i} \tag{3.19}$$

where n_i is the refractive index of the material in the shifted waves frequency. φ_1 and φ_2 can be determined using equation 3.10. If the crystal plane is depicted onto a detector the delay can be determined. Note that if $\varphi_1 = \varphi_2$ we get back the second harmonic generation case described in [10].

Chapter 4

Materials and methods

4.1 The Lund terawatt system

To generate the fs 790 nm pulses a the Lund Titanium Sapphire Terawatt laser system [11] was used. Two 532 nm Nd:Yag laser are used as pumping lasers for the Ti:Sa crystal. Through mode-locking and chirped pulse amplification system is used to generate 200 mJ sub 100 fs pulses at a 10 Hz repetition rate. A compressor was used to compress the pulses even further down to about 35 fs. In all experiments only a very small part of the total energy (less than 2 mJ) was used.

4.2 Experimental setup

This setup was based on the setup described in [10]. A beamsplitter first divides the beam roughly equally into two arms. The lower arm in figure 4.2 get further attunated by a neutral density filter for 790 nm so that the pulse energy could be controlled. Energies from 1-500 μJ were tested. The upper beam is focused by a lens (50 mm focal length) into a glaswindow in which a spectral broadening takes place. The beam is then made parallel by a second lens (50 mm focal length) and passes through a commercial attunation array which further reduced the intensity. Both beams are focused into a KDP crystal using a cylindrical lens (focal length 100 mm) which was angled for 340 nm phasematching. Two RG780 and UG1 filters absorption filters and a 340 nm interference filters were used to filter out the 340 nm beam. To detect the SFG beam a 180 mm focal length lens makes a 1:1 projection of the crystal onto a detector. The position is then measured as a function of the relative delay.

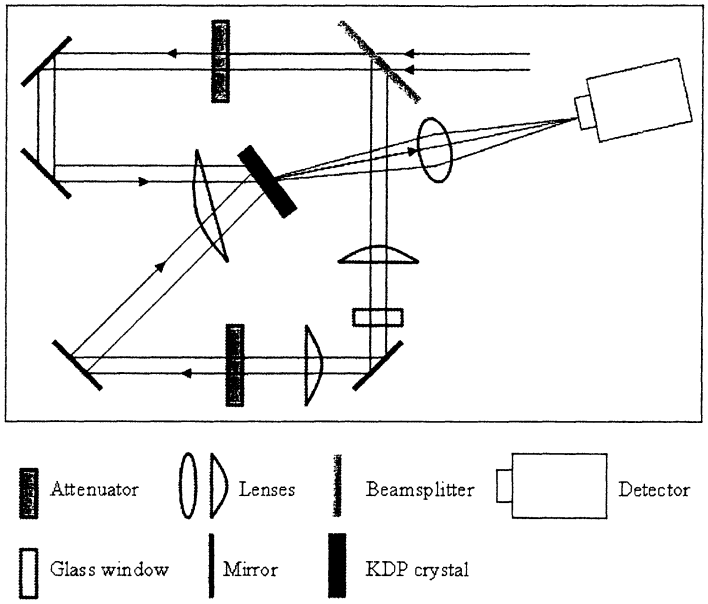

Figure 4.1: A sketch of the Lund setup

4.3 Detectors

Several detectors were used.

1. Alpha laser technology CCD-2000M (1-D CCD)
2. SiTek Electro optics PSD (Position sensitive detector)
3. Ueye 1440-M digital CMOS camera
4. Hamamatsu Orca
5. Hamamatsu Orca with image intensifier

4.3.1 Alpha laser technology CCD-2000M

The CCD consists of 2048 14×2000 μm pixel making up a 1-D array. The scanning rate ranges from 0.25 to 4 MHz. It can operated from an external power source or internal battery, thus the pixel array will show up as a time dependent signal on a oscilloscope. The spectral sensitivity range is 320-1100 nm.

4.3.2 SiTek Electro optics PSD

A position sensitive detector consists of a photosensitive area with a number of anodes at the edges. Depending on where on the detector the light signal

hits the current through the different anodes will vary with the distance to the anode. For a simple 1-D PSD only two anodes and thus output signals are used. The PSD has two voltage outputs V_1 and V_2, corresponding to the number of electrons collected at the different ends of the array. The relative position is given by $p = \frac{V_1}{V_1+V_2}$. In this experiment a SiTek Electro Optics PSD with an active silicon area of 10x2 mm was used. The main reason for using a PSD is because it has a very fast readout time compared to CCD detectors.

4.3.3 Ueye 1440-M digital CMOS camera

This CMOS camera has an USB interface and a resolution of 1280x1024 with a 6 μm pixel size. It is however at delivery fitted with a optical window that does not transmit 340 nm light which have to be removed for it to function properly in this setup.

4.3.4 Hamamatsu Orca

The Orca is a highly sensitive CCD camera with several additional features such as chip temperature control and pixel bunching that sets it apart from the other detectors. The Orca also gives a 2-d output through the firewire interface and is controlled with the Wasabi software provided by Hamamatsu. It has a resolution of 1344×1024 with a pixel size of 6 μm.

4.3.5 Image intensifier

The Hamamatsu image intensifier consists of a photo cathode, a micro channel plate (MCP) and a phosphorous screen. The photo cathode converts the few incoming photons into electron which are then multiplied in the MCP and at last converted back to photons by the phosphor screen. The phosphor screen is then depicted onto the orca display. The image intensifier can amplify light from 280 to 720 nm which is essential for the experiment. Many image intensifiers have windows that block out 340 nm radiation. It is controlled through a USB interface using a computer.

Chapter 5

Experiments

5.1 Aligning the setup

The setup is very alignment sensitive and to get a good result it is of the utmost importance that the system is aligned as good as possible. Coarse alignment is done by eye and by optimizing the signal on the detector. Keep the two beams in the same plane as the optical table throughout the setup and have the two pulses arrive at the same time (or within the scanning window). As describes below there are several other things that has to be considered for a finer alignment of the system.

5.1.1 600 nm generation

To generate an even 600 nm signal it is important to have the proper focus in the glass. The focus must not be too small (i.e. the lenses focusing the beam into the glass can't have too small a focal length) for it will then burn the glass and deteriorate the signal, any focal length above 50 mm should do fine. Of course this depends on the energy of the incoming beam and if you are using pulses of more than 500 μJ energy it might actually be wise to place the focus just after the glass or do self-phase modulation in air. The width of the glass plate should be at least 1mm, thinner plates generate less 600 nm light and also give rise to a fluctuating signal which will decrease resolution.

5.1.2 The cylindrical focus

When focusing the beams into the crystal it is of course vital that one achieves as good spatial overlap as possible between the two pulses. Using a slip of photosensitive paper it is easy to get a projection of the focus. This would seem to guarantee a good overlap in the crystal. However, since both beams can be considered to be gaussian it is also important that the

focuses do not lie to far apart from each other in the direction of propagation. If that should happen one wavefront will be curved with respect to the other which will result in a deterioration of the resolution as all parts of the beam will no longer meet at the same time. The signal could then appear to have a slight slant. On 2D array this this can be compensated by choosing to measure on a specific part of the beam but on a 1D array the resolution can be lowered by several 100 fs. Because of this, it is recommended that a 2-D detector is used for alignment.

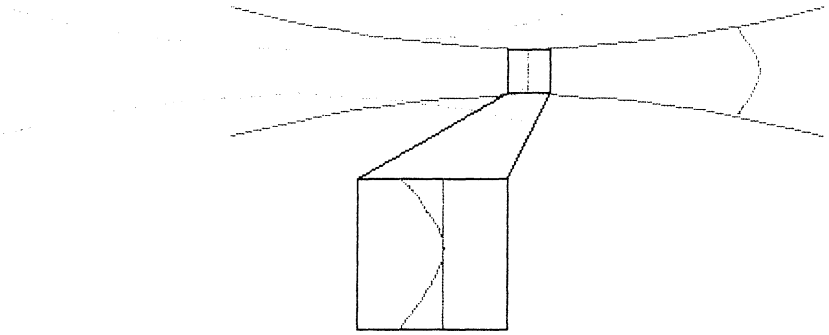

Figure 5.1: Wave fronts meeting in the crystal

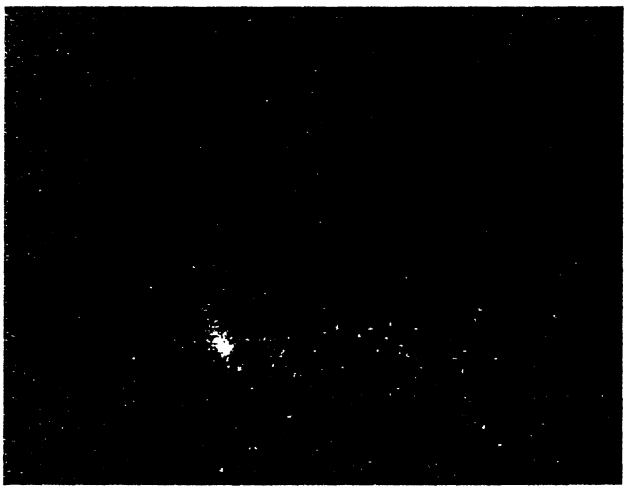

Figure 5.2: Measurement taken with Hamamatsu orca showing a tilted signal

5.1.3 Scanning range

As seen in figure 4.2 two lenses are used to focus the light into the glass and then make it parallel again. It is possible to shift the position of the second

lens a bit to control the spot size of the beam after self-phase modulation. This could allow you to focus all of the 600 nm photons into a smaller beam thus creating a stronger signal. However if the beam is made too small the measurement window will decrease and if the beam is not parallel the conversion efficiency could decrease due to the fact that not all parts of the beam would enter the crystal in the same angle and thus it would be hard to optimize the beam to the best phase-matching angle. A 5 mm diameter beam is enough for a scanning range of 6-7 ps.

5.2 White-light analysis

5.2.1 Spectra

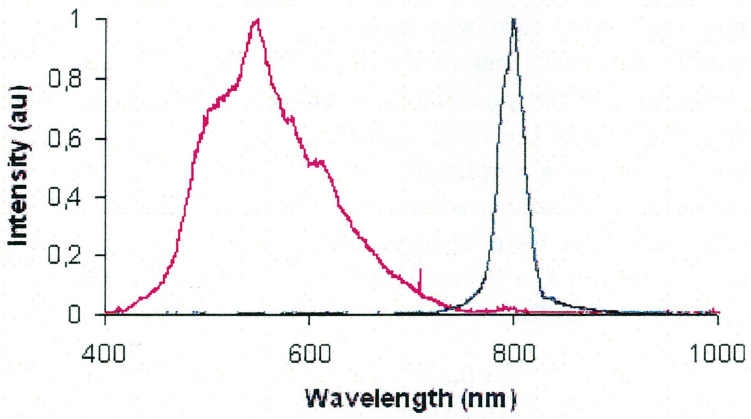

Figure 5.3: Normalized spectra with (pink) and without (blue) a RG790 filter

To measure the white-light spectra an Ocean Optics spectrometer connected to a computer was used. However it seems that only a very small portion of the light is partially transformed into 600 nm which made it very difficult to measure the 600 nm signal without using filters due to saturation in the spectrometer. When trying to study the light with a color filter that blocks everything above 790 nm we are basically just seeing the transmission curve of the filter. However it was not possible to study the region around 600 nm without a filter due to saturation in the spectrometer. One conclusion that can be drawn is that the lower limit lies around 480 nm and that the spectral intensity peaks around 500-650 nm.

5.2.2 Pulselength

By studying the spatial length of the signal on the Hamamatsu Orca we can use equation 3.18 to determine the 600 nm pulse length. After studying the signal we can determine that it is about 100 μm which gives a signal length of about 150 fs with the assumption that the 790 nm pulse is 45 fs. Simulations using code developed in [15] shows that the broadening from optical components is about 50 fs. However if a 600 nm interference filter is introduced to the setup this broadening is increased by as much as 1 ps. Thus it is recommended that absorption filters are used instead of interference filters to filter out the 790 nm component.

5.2.3 Intensity and conversion efficiency

Using a Hamamatsu photomultiplier tube the number of photons in the the self-phase modulated arm was measured. A 600 nm 40 nm FWHM interference filter was place before the PMT to ensure than only photons which can generate 340 nm photons through sum frequency are measured. The quantum efficiency of the PMT at 600 nm is 0.1. The PMT is operated at 600 V at which it has a amplification of $5 * 10^4$. A 15 ns 100 mV signal was measure on an oscilloscope using a 50Ω terminator when the signal was attenuated 10^6 times (the beam energy used to generate this light was about 1 mJ). The current can the be expressed as a function of the number of photons striking the detector:

$$I = \frac{e * n_e}{t} = \frac{V}{R} = \frac{1.6 * 10^{-19} * 0.1 * 5 * 10^4 * n_\gamma}{15 * 10^{-9}} = \frac{100 * 10^{-3}}{50} \rightarrow n_\gamma = 37500 \tag{5.1}$$

This gives that the number of photons before dampening to $4 * 10^{10}$. Since a 1 mJ 790 nm pulse contains about $4 * 10^{15}$ photons the conversion efficiency is 10^{-5}. More of less all of these photons can create light that can pass through the last 340 nm 10 nm FWHM interference filter. However, the phase matching condition will not allow all wavelengths to create a signal at the same time.

5.3 Sum frequency beam studies

The spectral shape of the 340 nm is solely determined by the range of filters it has passed through, but there are several other properties that is worth studying. The first is obviously the number of photons in the pulse. The SHG efficiency for the KDP crystal used was tested to check that crystal has not been damaged. A 790 nm signal was sent through and the number of photons after the crystal was measured with and without a color filter which removes all light above 790 nm. The conversion efficiency was found to be about 35%, note that this is for a single beam where the entire beam can

interact which genrally isnt the case. Using a UV-sensitive photomultiplier tube the 790/600 SFG efficiency was however found to be much lower, almost as low as 10^{-4}. Some of this can be blaimed on the filters involved, especially the 340 nm interference filter. Also the KDP crystal used was cut to fit 790 nm SHG rather than 790/600 SFG at a 12 degree angle which meant that it had to be tilted which might have affected conversion efficency. It is assumed that about 10% of the incoming beams could interact at a given delay and that roughly 90% of the SFG signal was lost in various filters before reaching the detector. This gives a per-pixel conversion efficieny of about 1%. Generally about 50 photons/pulse striking the image intesifier is enough to get a clear signal.

The second thing to study is the shape and spatial length of the signal. Sadly it is impossible to show moving media in a paper report but a film of the signal would show a constantly shifting signal without a clear center and several side signals. The signal also changes shape and size as the relative delay versus the 790 nm signal changes. Studies were made using 790 nm SHG which showed that these effects are not inherent to the optics but are parts of the self-phase-modulation process. As such, they can not be expected to appear in a application that does not involve a white light generated 600 nm signal, such as a FEL. The spatial size of the signal is about 100 μm, which is about 30 μm bigger than it should be it both pulses had undergone no temporal stretching.

The third thing that could be noted is that at high energies a lot of pre/post pulses could be observed which is shown as additional signal right and left of the original signal on the detector. These side pulses were separated form each other and the main pulse by about 1 ps and only showed up when aligning the setup. As soon as the signals were dampened down they disappeared, they were found to be about 10^3 times weaker than the main pulse. Again, these 'sidebands' could not be seen when running 790+790 nm SFG.

5.4 Resolution studies using the Hamamatsu Orca with image intensifier

5.4.1 Setting

All measurements in this section is done using the Hamamatsu Orca at maximum gain (255) connected a UV-sensitive gated image intensifier running at 999V (maximum setting).

5.4.2 Signal

The 340 nm photons generated in the crystals were filtered through three different filters before striking the image intensifier. Two RB780 and UG1 absorption filter were used to eliminated 400 and 790 nm light which can drown the signal at low intensities. The 400 light comes from SHG in the strong IR beam which can be refracted in the surface of the crystal and combined with itself. Last a 340 nm 10 nm FWHM interference was used to filter out any stray light. It should be noted that this filter only has a transmission of 50% at 340 nm but is neccessary for using the image intensifier. A sample of the signal on the Hamamatsu Orca is shown in picture 5.4.2.

Figure 5.4: Example of the signal on the Hamamatsu Orca

5.4.3 Measuring the position

To determine the consistency of measurements several shots were take in the same position and the peak position determined. Using $\phi_1 = 6.13$ degrees and $\phi_2 = 8.27$ (as shown in picture 3.2) degrees we get using equation 3.18 that one pixel on the detector (using 2x pixel bunching) correspond to about 16 fs. The time scale below is relative to the smallest (left-most) measurement. The reason the position is not the same for all measurements is that the self-phase modulated signal is constantly fluctuating, by doing continuous measurements you can see the signal shifting. The peak position of 20 consecutive pulses was measured and plotted relative to each other for two different beam energies as shown below.

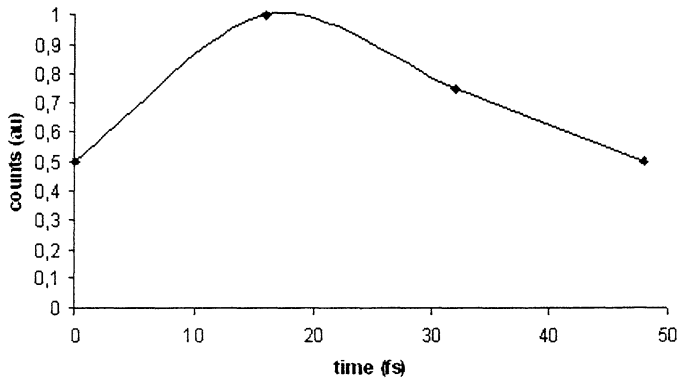

Figure 5.5: Position measured with $< 4 * 10^6$ photons in the self-phase modulated arm.

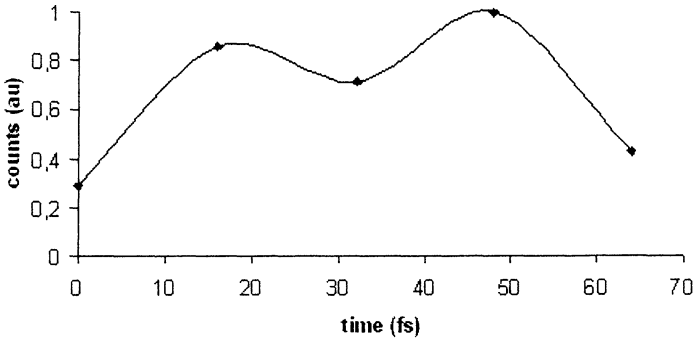

Figure 5.6: Position measured with $< 10^6$ photons in the self-phase modulated arm.

5.4.4 Time series measurements

To determine at what precision this method can measure the pulses a delay stage was mounted to shift the horisontal positions of the upper leftmost mirrors in picture 4.2.

The time delay introduced by this stage is:

$$\Delta t = \frac{2\Delta L}{c} \tag{5.2}$$

This time delay was the compared to the position and corresponding time delay measured by the Orca. To calculate the relative delay from the signal position on the ORCA equation 3.18. Several series were made at different energies to determine how the precision varies with the number of photons in the two arms. Least square linear regression was used to create a calibration curve to which the results were compared. The difference between the measurements and the calibration curve was then plotted. Time series and error plots for different energies are shown below.

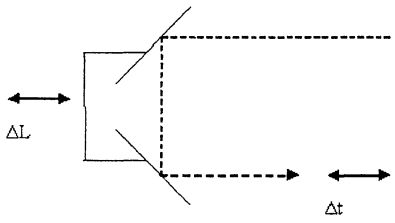

Figure 5.7: Sketch of the delay stage

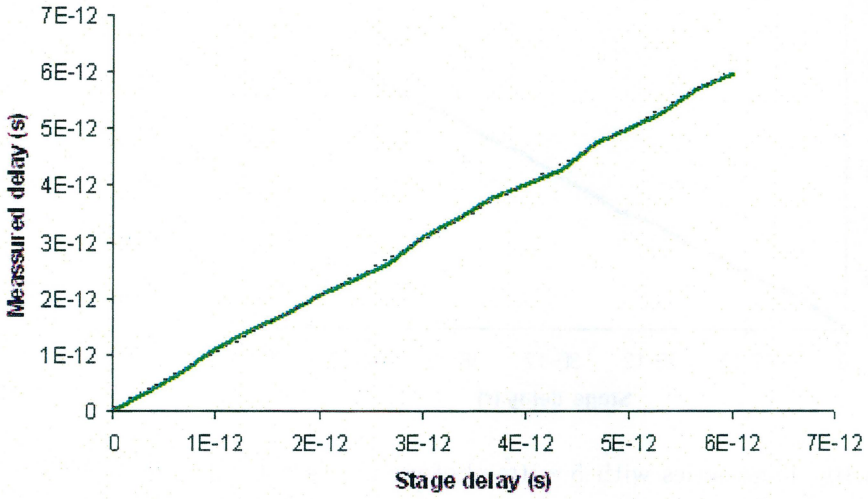

Figure 5.8: Time series with $5 * 10^6$ photons in the 600 nm arm and 10^{14} in the IR arm. The green line represents the time delay introduced by the delay stage plotted against the delay measured on the ORCA. The dotted line represents the calibration curve.

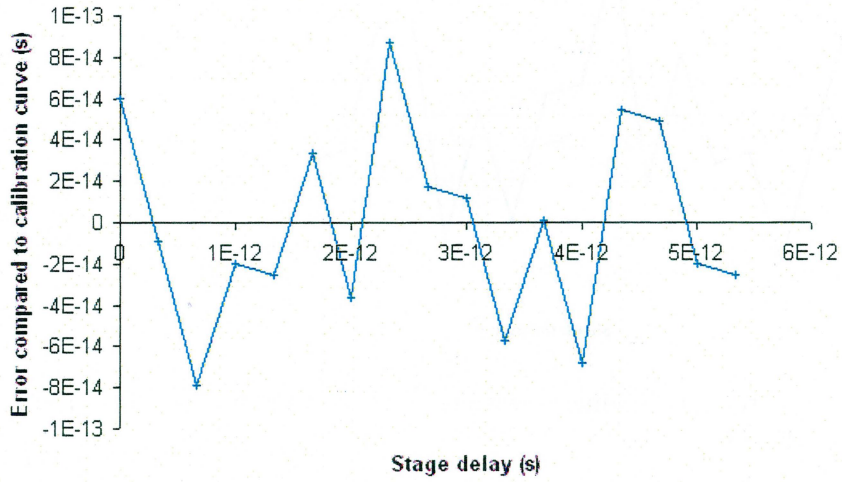

Figure 5.9: Error measurements with $5 * 10^6$ photons in the 600 nm arm and 10^{14} in the IR arm

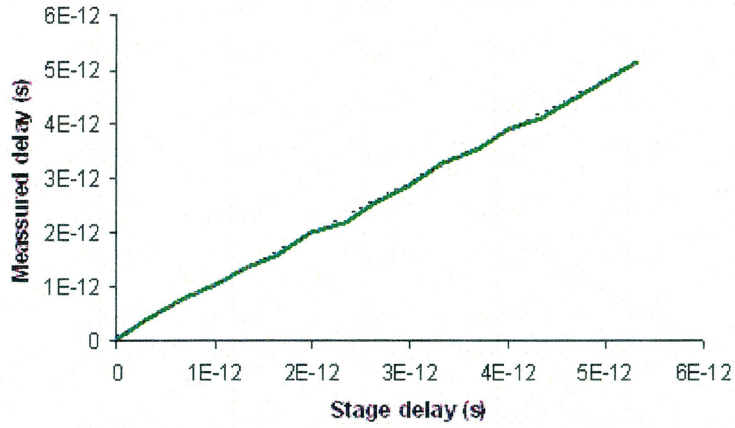

Figure 5.10: Time series with $5 * 10^5$ photons in the 600 nm arm and 10^{14} in the IR arm. The green line represents the time delay introduced by the delay stage plotted against the delay measured on the ORCA. The dotted line represents the calibration curve.

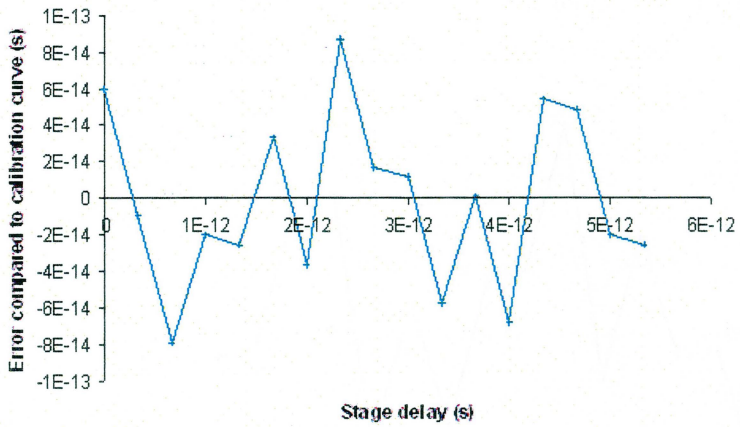

Figure 5.11: Error measurements with $5 * 10^5$ photons in the 600 nm arm and 10^{14} in the IR arm

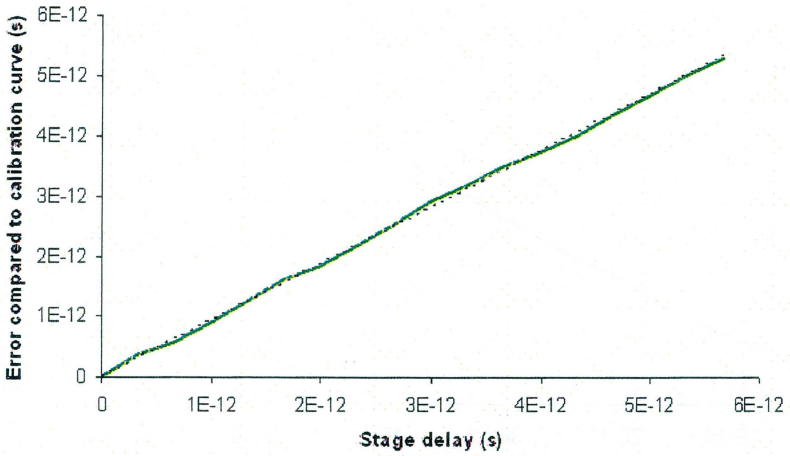

Figure 5.12: Time series with $5 * 10^5$ photons in the 600 nm arm and 10^{15} in the IR arm. The green line represents the time delay introduced by the delay stage plotted against the delay measured on the ORCA. The dotted line represents the calibration curve.

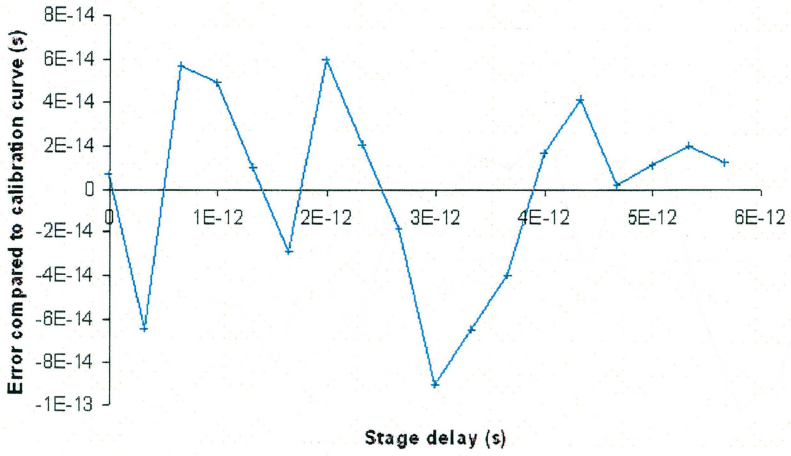

Figure 5.13: Error measurements with $5 * 10^5$ photons in the 600 nm arm and 10^{15} in the IR arm

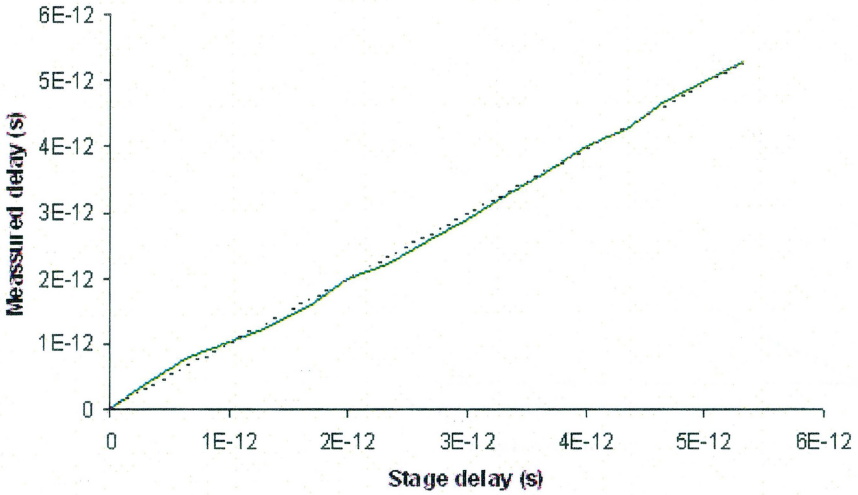

Figure 5.14: Time series with $1.5 * 10^5$ photons in the 600 nm arm and 10^{15} in the IR arm. The green line represents the time delay introduced by the delay stage plotted against the delay measured on the ORCA. The dotted line represents the calibration curve.

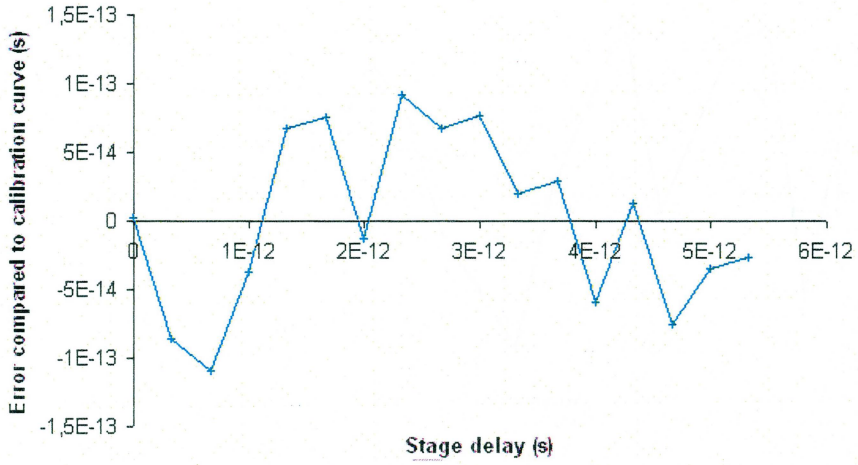

Figure 5.15: Error measurements with $1.5 * 10^5$ photons in the 600 nm arm and 10^{15} in the IR arm

5.5 Resolution studies using the other detectors

5.5.1 Resolution for pixel-type detectors

Most of the detectors that were used here work in about the same way. A signal is recorded on some kind of pixel array (1D or 2D) and the result is then read on a oscilloscope or computer. As such the resolution on these kind of devices are solely dominated by the size of the signal and the pixel size of the detector. In all cases studied (The CCD and Ueye cameras) the accuracy of which the position of the signal could be determined was identical to that of the Orca. This was expected since the Orca itself was used with as much as 4x pixel-bunching corresponding to a pixel size of about 25 μm (or 30 fs) without an increase in read-out error.

The 1-D CCD array proved to be the noisiest of the detectors. This noise comes primarily from three sources: stray light, power supply and internal amplification. Even with the 340 nm filter at the end some light manages to get through to the detector. This can be countered by shielding the detector from all sides in several layers. The power supply also induces some noise which can be countered by purchasing a stable power supply. The last and worst form of noise seems to come from the amplification system in the detector since it grows with the size of the signal. This limited the its sensitivity.

5.5.2 Resolution for the PSD

For the position sensitive detector a full time series was made to analyze the accuracy of which a delay could be measured. The voltage difference $\frac{V_1-V2}{V_1+V_2}$ was plotted as a function of the delay after background had been subtracted.

The so called linear area [10] can be identified as the area between the highest and lowest value in the plot (not general case). For this area a calibration curve is made and relative errors were found to be as much as 1 ps in some cases. Without amplification and other screening the PSD was deemed not suited for further experiments.

5.6 Sensitivity

One of the main goals of this experiment was to determine at how low intensities a SFG autocorrelator could function. As mentioned above, these numbers are also tied to the range one wishes to study. For the ranges studied above the smallest energies for which the signal could be observed and its position measured is shown in the table below.

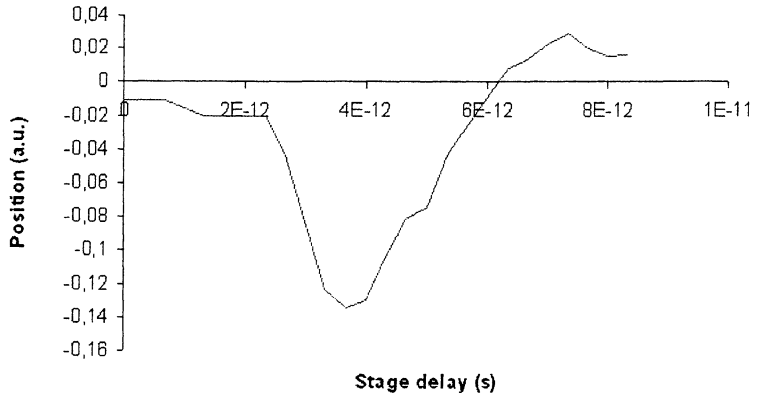

Figure 5.16: Time series measurements with 10^9 photons in the 600 nm arm and 10^{15} in the IR arm using the PSD

Detector	*IR photon count/pulse*	*600 nm photon count/pulse*
Hamamatsu Orca with image intensifier	$10^{15}/10^{14}$ (200/20 μJ)	$1.5 * 10^5/5 * 10^5$
Hamamatsu Orca	10^{15}	$5 * 10^7$
Alpha laser technology CCD-2000M	10^{15}	10^9
SiTek Electro optics PSD	10^{15}	10^9
Ueye 1440-M digital CMOS camera	10^{15}	10^9

All of these results were done with a resolution of 100 fs or better. Higher IR pulse energies can not be used without causing white-light generation in the crystal, which could damage it.

5.7 Error analysis

As shown in the time series plots the errors when measuring the position of the signal is about 50 fs. This error can be contributed to the changing nature of the signal which in turn can be trace to the white-light generation. Some part of this error can be expected to disappear in an implementation without a white-light generated 600 nm beam.

Another error that is introduced but does not really affect the method is the error in the simulated time delay of the delay stage. The delay stage has a micrometer screw where each step corresponds to 10 μm. Each measure-

ment point was taken 50 μm apart corresponding to a difference of about 300 fs. The error is estimated to be less than 10% of that; 30 fs.

Faulty depicting of the focus in the crystal would give a non-linear response, that is the signal would move a different amount depending on where it was. However the errors compared to the linear calibration curve seem to be random in sign and size so no conclusions about this can be drawn. Also experiments were done to ensure that the optics used to depict the focus could properly depict μm structures.

Beam geometry is another error. If the beams don't travel in the same plane or are not focused in the same plane all equations have to be rewritten. Again these errors can be seen as be traced back from the signal, such as the slanting signal problem described above.

Chapter 6

Comparative techniques

There are already several established methods for measuring jitter in FEL installations. The two most common is described below.

6.1 Streak cameras

A streak camera consists of a photo cathode or similar device that converts incoming photons into electrons. These electrons then pass through a time-varying electric field perpendicular to their original trajectory. If two photons hit the photo cathode with a time difference of δt then the subsequent generated electron will be subject to different electric fields and thus be be deflected in different angles. By detecting these electrons and knowing the electric field the time difference δt can be computed. Streak cameras typically has a resolution of a few hundred fs [12] and can detect pulses containing no more than a couple of photons. However apertures constrict a streak camera in such a way that can have a good resolution and a good sensitivity, but not at the same time. Also they tend to be relatively expensive, costing in the range of several million swedish crowns [12].

6.2 Electro-optical sampling (EOS)

In contrast to other techniques EOS uses the electron bunches in the accelerator to measure the timing. A densely compressed pulse of electrons moving at relativistic speeds has a very strong transverse electromagnetic field. This strong field will distort the refractive index of nearby optical media. A crystal is placed near the beam pipe and a laser pulse is sent through it at an angle. If the electron bunch passes by at the same time as parts of the laser pulse is inside the crystal then the polarisation of the photons in the crystal will be aligned to the electric field of the electrons. The signal is then filtered through a polarizer and the remaining part is detected. If the electrons passes at different time from pulse to pulse different parts of

the laser pulse will be in the crystal and thus the relative jitter can thus be detected. Electro optic sampling has a resolution of about 60 fs [13]. The downside of this method is that it has to implemented near the beamline with can be consider cumbersome compared to other methods. EOS can be considered to be as costly as a streak camera.

Chapter 7

Conclusions

7.1 Sensitivity and resolution

With a correctly aligned setup the Hamamatsu Orca with an image intensifier can deliver delay measurements with a 100 fs accuracy at 600 nm photon counts less than 10^6 photons/pulse. Every pixel-based detector with a pixel-size less than 25 μm should was found to deliver the same accuracy. Cheaper CCD and CMOS cameras without image intensifiers can be expected to go as low as 10^9 600 nm photons/pulse. When going toward 10^5 photons/pulse the signal has to be more centered to be observed. The errors relative to the calibration curve seem random and thus it is concluded that it is possible to obtain a good calibration by hand.

7.2 Comparison with other techniques

The main advantage of the method developed here is that its relatively cheap and very accurate. The detector sets the price for the setup, the rest of the components cost nothing compared to it. Even an expensive detector such as the Hamamatsu Orca with an image amplifier is a factor 10 cheaper than a streak camera and can provide a better resolution. The time resolution can not quite match that of the EOS however since much uncertainty comes from the self-phase modulation process which wont be present at a FEL it is probable that the resolution can improved further. For strong FELs with high beam dump photon counts cheaper detectors can be used which can reduce the cost to a couple of thousand swedish crowns. The setup further only requires a stable optical table to stand on and 1x1/2 meters of space. Using a gated image intensifier the system could be operated under normal light conditions.

7.3 Further improvements

One big disadvantage of using CCD monitors to read the signal is that they cant provide information at a very fast rate. Even the best cameras can not deliver more than ten or twenty pictures per second. For a free electron laser pulse train where pulses are separate by less than a picoseconds this only allows you to make a single measurement per train. This was not a problem in the setup since a 10 Hz Ti:Sa was used to in a real life implementation this would be a severe limitation. As seen above this experiment was unable to provide satisfying results using a PSD. However it can be seen that in [10] where a system of amplifiers was used to clean up the signal much better results were obtained, although at higher photon counts. By combining an image intensifier with a PSD and provided than optical laser pulses can be provided at the same rate this problem could be solved. This is because the PSD readout time is much faster than a CCD. The PSD is also better suited for closed circuit implementations such as automatic feedback control systems where you don't want a time-dependent scan signal but rather an instant measure of the position.

The KDP crystal used in this experiment was cut for 790 nm SHG, not for SFG with 790/600 nm beam intersecting at 12 degrees. This meant that the crystal has to be slanted to achieve good phasematching conditions. Even if this did not induce any problems it would be recommended to order a crystal specifically cut for the purpose of a permanent setup.

7.4 Comments on the experiment

The goal of this diploma work was to develop a method for FEL jitter measurements that was compact and as cheap as possible. SFG is today not widely use at FEL because it is believed to not be able to provide good enough resolution at low intensities [14]. The TTF as Desy, Hamburg provided that such a technique should at least be able to handle SFG generation at 20μJ IR pulses with 600 nm photon counts of less than 10^6 photons per pulse. These requirements were used as a base for the experiment. It was first believed that this could be achieved with the 1-D CCD and PSD detectors but SFG conversion efficiency proved to be much lower than expected.

It was originally planned that the final setup should be implemented at the TTF but this was made impossible due to time delays.

This experiment was unable to reproduce the result achieved in previous work [10] especially where photon counts and conversion efficiencies were

concerned. In [10] weak arm to signal conversion efficiencies of 35% were meassured. As in most cases only about 10% of the weak beam is interacting with the strong beam such converion efficiencies was found impossible to obtain. Also filter calibartion and resolution studies gave different results.

Chapter 8

Acknowledgments

First and foremost of all I would like to thanks my supervisor Jörgen Larsson and all other members of the ultrafast x-ray science group without whom I would not have gotten very far. I would especially like to thanks Ola Synnergren and Henrik Engquist who have gone out of their way to help me several times.

Secondly I would like to thank all members of the division of atomic physics a LTH. A special thanks goes out to Emelie Pourtal and Anders Persson who always solved every laser related problem I ran across with a smile and Olivier Guilbaud who were very patient with me during times when I needed alot of beam time.

Last but no least I thank my fionce Sara Bergström for her loving support through rainy days.

Bibliography

[1] http://www.osmic.com

[2] http://xfelinfo.desy.de

[3] http://www.xfel.net

[4] Freund and Antonsen *Principles of Free-electron lasers* Chapman and Hall 1996.

[5] Sverker Werin *Undulator physics and coherent harmonic generation at the MAX-lab electron storgae ring* LUNDTDX/(NTMX-1002)/1-207/(1991)

[6] Gil Travish *Experimental Requirements for a Self-Amplified Spontaneous Emission Test System: Design, Construction, Simulation and Analysis of the UCLA High Gain Free Electron Laser* Ph.D. Physics (Beam) - UCLA 1996 http://www.myaxys.com/travish/dissertation.html

[7] Robert W. Boyd *Nonlinear optics - second edition* Academic press 2003.

[8] Orazio Svelto *Principles of lasers* Plenum press 1998.

[9] Robert R. Alfano *The Supercontinuum Laser Source* Springer 1989.

[10] V Tenishev, V Acdeichikov, A persson and J Larsson *On-line diagnostic tools for measurement of the time delay between two ultrashort light pulses* online stacks.iop.org/MST/15/1762

[11] S Svanberg, J Larsson, A Person and C-G Wahlström *The Lund high-power laser facility* Phys. Scr. 49 187-97

[12] http://www.hamamatsu.com

[13] A.L Cavalieri D.M Fritz S.H lee P:H Bucksbaum D.A Reis and others *Clocking femto-second x-ray* Physical review letters PRL 94, 114801 (2005)

[14] Jörgen Larsson private conversation

[15] Anna Engström *Generation of ultrashort laser pulses through filamentation* Lund reports on Atomic Physics LRAP-357 Lund May 2006

Appendix A

The final setup

Items used for the final setup

1. 1 optical table
2. 1 beamsplitter
3. 1 attunation array
4. 4 25mm diameter silver mirrors
5. 1 Thorlabs 340 nm 10 nm FWHM interference filter
6. 1 RG790 color filter
7. 1 UG1 color filter
8. 2 25mm diameter 50 mm focal length lenses
9. 1 50mm diameter 100 mm focal length elliptical lens
10. 2 50mm diameter 180 mm focal length lens
11. 3 25mm diameter mm glass plate
12. 1 delay stage
13. Hamamatsu Orca with image intensifier
14. Various appertures, lenseholders and screws

Items used for experiments and testing

1. 1 Thorlabs 600 nm 40 nm FWHM interference filter
2. 1 Acer travelmate 370 laptop with USB and firewire connectors
3. 1 Textronic oscilloscope

4. 1 Hamamatsu photomultiplier tube (sensitive at both 340 and 600 nm)
5. 1 USB2000 Ocean optics spectrometer
6. various coaxial and power cables

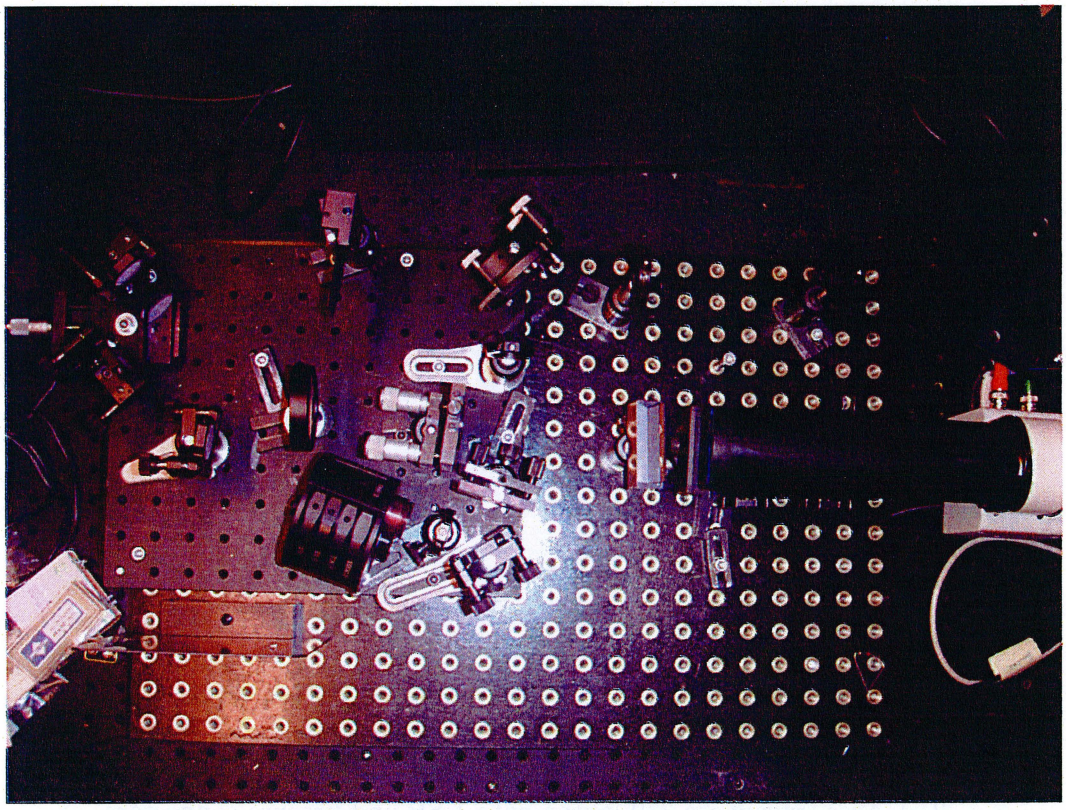

Figure A.1: A picture of the setup